ALONG TRACK SLOPE COMPENSATION IN A SIMO FORMATION

Naomi Petrushevsky, Andrea Monti-Guarnieri

Politecnico di Milano
Department of Electronics, Information and Bioengineering
Via Ponzio 34/5, 20133 Milan, Italy

ABSTRACT

Compact single-input-multiple-output (SIMO) formations are a promising option for performance improvement in future Synthetic Aperture Radar (SAR) missions. A high-resolution unambiguous imaging is obtained by utilizing several satellites with small antennas. The across-track baseline between the satellites poses a significant issue for known signal reconstruction algorithms due to the dependency on the topography, which may vary along-track. Proposed here is a method to compensate for height variations along the azimuth direction using a simplified but powerful 1-D model. A theoretical derivation of a forward model is provided, and performance analysis in terms of signal to noise is demonstrated.

Index Terms— SAR, Multi-channel image formation, SIMO, Across-track baseline, Topography.

1. INTRODUCTION

In recent decades, spaceborne SAR systems have proven their outstanding capabilities in providing insights about various phenomena on Earth's surface and surrounding atmosphere. Further performance improvement can be obtained in the future by exploiting SIMO formations [1, 2].

The usage of several satellites allows to reduce the antenna size (i.e., improved resolution) without the need to increase the Pulse Repetition Frequency (PRF), which conditions the swath size. Each satellite is under-sampling the azimuth spectrum, resulting in ambiguities. However, by properly combining the signals from all sensors, one can recover the entire spectrum without aliasing [3, 4].

In the context of a SIMO formation, some degree of across-track (XT) baseline between the satellites is inevitable due to orbit control capabilities. The XT baseline translates to a phase difference between the channels, which depends on the topography. This additional phase interferes with the proper signal reconstruction, leaving uncompensated residual ambiguities [5, 6].

The mitigation of ambiguities in such case is not yet fully solved in literature. Compensation of a non-zero XT baseline was demonstrated in [7], but the proposed solution assumed a flat earth, which does not fit the general case. Elevation variations were considered in [8], but only in the range direction, not handling topography changes along the azimuth.

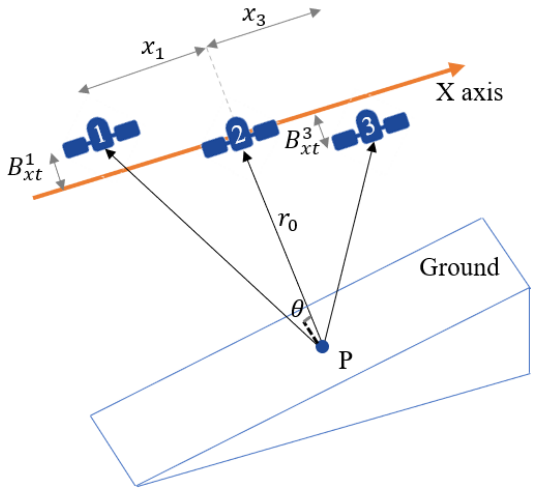

Fig. 1. Simplified geometry of a SIMO formation: targets are assumed lying on a constant slope along-track.

This article aims to provide a framework for combining the channels of the SIMO system described in Fig. 1, accounting non-zero XT baselines. This solution assumes that a slope can describe the topography along the azimuth. The simplification does not cover all real use cases, but it is a significant improvement w.r.t a flat terrain model. To analyse the signal reconstruction algorithm, a 1-D model along-track is discussed, and performance are investigated. However simple, it holds the key elements of the problem and can be extended to the case of a fully operational SAR.

2. FORWARD MODEL

Let us consider a signal d_0 which is observed by a single SAR system with the following Pulse Repetition Frequency (PRF):

$$f_{prf} = \frac{2v}{L_a}\zeta \Rightarrow \zeta = \frac{f_{prf}}{2v/L_a} \tag{1}$$

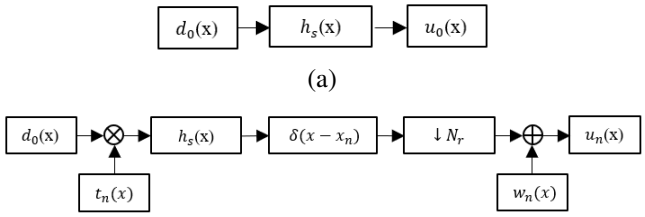

Fig. 2. Forward models of (a) properly sampled signal (b) down-sampled signal.

where L_a is the length of the antenna. The term ζ is the ratio between the PRF and the antenna bandwidth, that is the oversampling for a conventional SAR: the larger the better for ambiguity suppression [5]. The transformed impulse response function of the SAR system can be approximated as:

$$H_s(k_x) = G_a(k_x)e^{jr_0\frac{k_x^2}{4\cdot\Omega_0}} \tag{2}$$

where G_a is the antenna pattern, k_x is the wavenumber, and $\Omega_0 = 2\pi/\lambda$, λ being the wavelength of the carrier. A 1D approximation is considered, assuming slant range r_0. The signal observed by the system in Figure 2.a (u_0) represents the raw data from a properly sampled SAR. The spectrum of u_0 is limited by the antenna: $k_x \in [-\frac{2\pi}{L_a}, \frac{2\pi}{L_a}]$, and then repeated periodically.

The role of the formation is to obtain u_0 from the observations of N sensors, each acquiring with a N_r times reduced PRF:

$$f_{prf}^n = \frac{f_{prf}}{N_r} \tag{3}$$

The reconstruction of a full band signal from a set of decimated versions of itself is possible only if a proper shift is introduced before down-sampling, as illustrated in Fig. 2.b.

In the case of the formations, each decimated raw data is acquired by a different sensor that is displaced across-track by B_{xt}^n w.r.t the reference, annotated in Fig. 1. This introduces a multiplicative phase screen to the observed scene that can be modeled as follows:

$$t_n(x) = e^{jC_n[q_0+q_1\cdot x]} \tag{4}$$

where q_0 is the average height of the scene in meters, and q_1 is the slope along azimuth. $C_n = \frac{2\pi B_\perp^n}{\lambda r_0 \tan(\theta)}$, being $B_\perp^n$ the component of B_{xt}^n perpendicular to the line-of-sight, and θ is the incidence angle. We do not address the range-dependant flat-earth phase since it was previously discussed in literature [7, 8]. The phase screen $t_n(s)$ is a modulation that shifts the scene's spectrum, and adds a constant phase:

$$D_n(k_x) = D_0(k_x) * T_n(k_x) = D_0(k_x - C_n q_1)e^{jC_n q_0} \tag{5}$$

Reducing the sampling rate by N_r causes aliasing. The

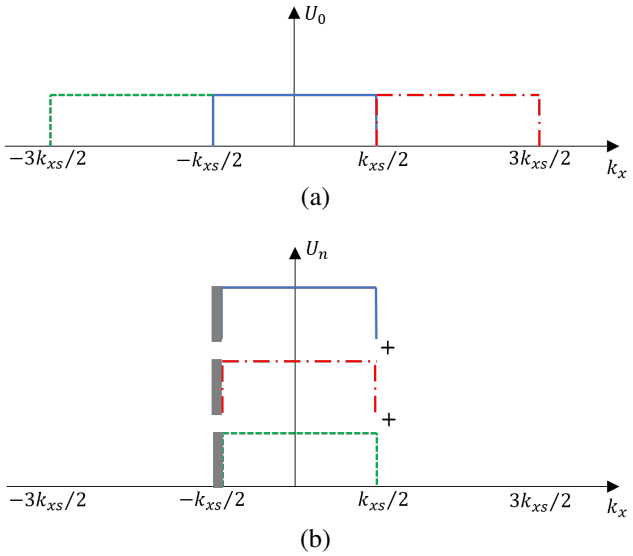

Fig. 3. Spectra of the (a) reference signal and (b) one down-sampled channel where $N_r = 3$, so three contributions are summed for each frequency. The grey blocks denote spectral components which contribute to the noise, due to the wavenumber shift.

folded signal is modeled in the frequency domain:

$$\begin{aligned} U_n(k_x) &= \sum_{i=0}^{N_r-1} U_0(k_x + ik_{xs}) \\ &= e^{jC_n q_0} \sum_{i=0}^{N_r-1} D_0(k_x - C_n q_1 + ik_{xs}) H_s(k_x + ik_{xs}) \\ &\cdot e^{jx_n(k_x+ik_{xs})} + W_n(k_x) \end{aligned} \tag{6}$$

where W_n is the spectrum of the noise, and $k_{xs} = 4\pi\zeta/(L_a N_r)$ is the sampling angular frequency. U_n is repeated periodically every k_{xs}.

The spectra of u_0 and u_n for $N_r = 3$ are illustrated in Figure 3.b. The spectral folds give rise to ambiguities in the focused data, and increase the clutter.

3. SIGNAL RECONSTRUCTION

3.1. Flat earth approximation

As a first-order approximation, one may neglect the effect of the slope q_1, and compensate only the constant term q_0 [8]. In this case the forward model reduces to:

$$U_n^{flat}(k_x) = e^{jC_n q_0} \sum_{i=0}^{N_r-1} U_0(k_x + ik_{xs}) e^{jx_n(k_x+ik_{xs})} \tag{7}$$

Given $n = 1, \dots N$, the linear system in 7 can be solved if $N > N_r$, i.e., the number of sensors is larger than the number of frequency folds. The minimum mean squared error

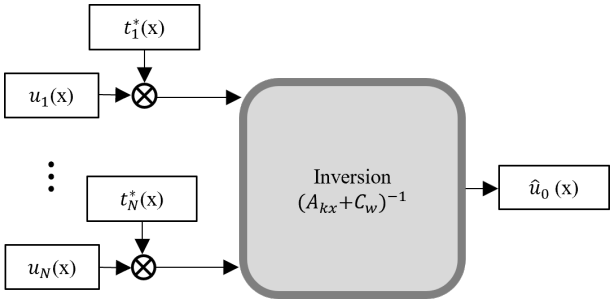

Fig. 4. Multi-channel slope compensation system.

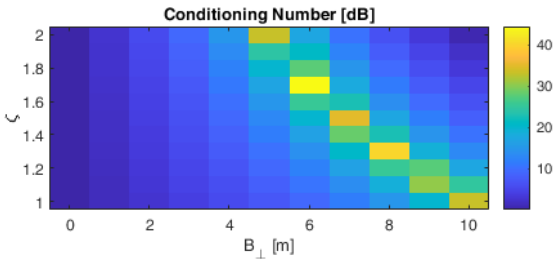

Fig. 5. Conditioning number of the matrix A_{kx} (13) as function of the normal baseline and the SAR oversampling.

(Wiener) solution is [4]:

$$\begin{aligned}\widetilde{U}_0(k_x) &= A_w A_{q0}^* U(k_x) \\ A_w &= A_{kx}\left(A_{kx}^* A_{kx} + C_w\right)^{-1}\end{aligned} \tag{8}$$

where U is a $N \times 1$ vector of observations, and A_{q0} is a diagonal matrix with the constant phase terms from 4. A_{kx} is an $N \times N_r$ matrix describig the spectral folds:

$$A_{kx} = \begin{bmatrix} e^{jx_1 k_x} & \dots & e^{jx_1(k_x+(N_r-1)k_{xs})} \\ \vdots & \ddots & \vdots \\ e^{jx_N k_x} & \dots & e^{jx_N(k_x+(N_r-1)k_{xs})} \end{bmatrix} \tag{9}$$

The covariance of the signal was assumed to be white and unitary, and C_w defines the covariance matrix of the noise.

While improving the overall signal-to-noise ratio (SNR), the solution 8 cannot completely suppress ambiguities when an along-track elevation slope is present. The performance of the approach is presented in Section 4.

3.2. Slope Compensation

To recover U_0, given a non-zero XT baseline, we process N channels with the inverse system described in Fig. 4. First, we apply the phase matched to $t_n(x)$ to each channel. The signal of sensor n (6) comes to be:

$$\begin{aligned}U_n(k_x) * T_n^*(k_x) = \sum_{i=0}^{N_r-1} D_0(k_x + ik_{xs}) \\ \cdot H_s(k_x + C_n q_1 + ik_{xs}) \cdot e^{jx_n(k_x+C_n q_1+ik_{xs})}\end{aligned} \tag{10}$$

Note that the shifted chirp in 10 can be expressed as:

$$H_s(k_x + C_n q_1) = H_s(k_x) e^{jD_n(k_x)} \tag{11}$$

where $D_n = \dfrac{r_0}{2\Omega_0} C_n q_1$, and a term with q^2 was neglected. By combining 10 and 11 we obtain:

$$\begin{aligned}U_n(k_x) * T_n^*(k_x) = \sum_{i=0}^{N_r-1} U_0(k_x + ik_{xs}) \\ \cdot e^{jx_n(k_x+C_n q_1+ik_{xs})} e^{jD_n(k_x+ik_{xs})}\end{aligned} \tag{12}$$

To get U_0, the system in 12 can be inverted similarly to (8), but the elements of the design matrix are:

$$A_{kx}^{j,i} = e^{jx_j(k_x+C_n q_1+ik_{xs})} e^{jD_j(k_x+ik_{xs})} \tag{13}$$

The result of the inversion is the estimation of the properly sampled raw data $\widetilde{u}_0$. At this point, azimuth compression can be applied to obtain an estimate of d_0.

3.3. Noise Amplification

By aligning the spectra of the different channels we implicitly apply a circular operator. Parts of the spectrum will be misplaced and will contribute to the noise, as depicted in Fig. 3.b by grey blocks. The noise power for those frequency bins is as high as the signal (unitary).

The stability of the solution depends on the parameters of the system. An upper boundary of noise amplification is estimated by the conditioning number (CN) in Fig. 5, given the system described in Table 1. Note that the first column refers to the flat earth approximation, which is not able to properly compensate ambiguities, but has a favorable CN. For certain combinations of baseline and PRF, the conditioning number becomes very high, i.e., the matrix is ill-conditioned. Thus, the across-track baseline should be limited according to the chosen PRF. An evaluation of the achievable SNR as a function of baseline and PRF is provided in Section 4.

In the analysis so far, we have assumed that the antenna acts as a perfect low-pass filter, eliminating any wavenumber higher than $2\pi\zeta/L_a$. In reality, the antenna pattern follows the following rule:

$$G_a(k_x) = \mathrm{sinc}^2\left(\frac{\Psi L_a}{\lambda}\right) = \mathrm{sinc}^2\left(\frac{k_x L_a}{4\pi}\right) \tag{14}$$

A choice of the operational f_{prf} will determine which part of the energy of u_0 is not accounted for in the proposed model, as shown in Fig. 6. Given the perfect along-track sampling and no XT baseline, the high-frequency components of the signal will cancel each other, and no ambiguities will arise. In the presence of an across-track baselines, the components contribute to the noise.

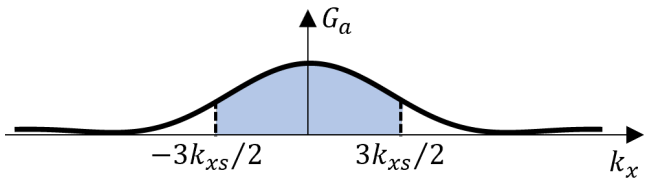

Fig. 6. Unfolded antenna pattern for three footprints. The central part (marked in blue) is covered by the proposed model. Higher frequencies are not considered, and act as additive noise.

Table 1. Simulated system parameters

Parameter	Symbol	Value
Carrier frequency	f_0	9.6GHz
Reference slant range	r_0	570km
Incidence angle	θ	30°
Number of sensors	N_r	3
Terrain slope	q_1	500m/footprint
single SAR SNR		30dB

4. RESULTS FROM SIMULATIONS

The acquisition of a sloped terrain by three channels was simulated, following the model in 2. The parameters of the system and geometry are summarized in Table 1. XT baselines were assumed symmetric w.r.t the central sensor ($[-B_\perp, 0, B_\perp]$, simulating the worst case scenario. Along-tack baselines are considered to be ideal, as suggested in [1].

The effect of the sloped topography depends on the position of the target. To evaluate the performance of the proposed algorithm w.r.t an entire scene, we simulated a uniform distributed target, i.e., a homogeneous white speckle. We then measure the SNR of the reconstructed signal in two cases: under the flat earth approximation from Section 3.1, and using the slope compensation described in Section 3.2. SNR is measured by:

$$SNR = \frac{1}{1-\gamma} \tag{15}$$

where γ is the amplitude of the correlation coefficient between the reconstructed signal and the ideal one, u_0. Additive noise was applied to the data, and the SNR of a single SAR is reported in Table 1. Fig. 7 shows the achieved SNR for different values of baseline and PRF (defined by ζ, as in 1).

In the case of no baseline, we obtain the ideal combination with both methods, where the gain w.r.t a single SAR is N. As the baseline grows, it is clear that the flat-earth approximation results in significant clutter. This is predictable, since the approach does not take into account the phase variation due to topography. The proposed method, which directly handles the slope in the inversion, performs better in suppressing ambiguities, even as the baseline increases. However, the operational region of the method is limited by the pairing of across-track baseline and PRF.

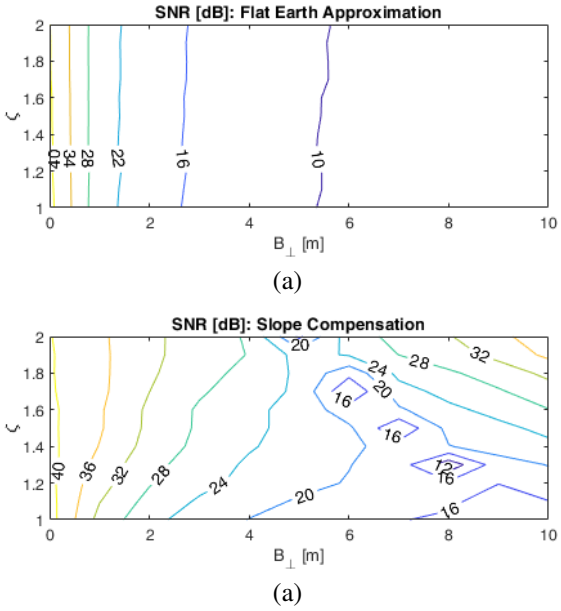

Fig. 7. SNR of reconstructed signal, accounting for both ambiguities and noise. (a) Flat earth approximation (b) slope compensation.

For small baselines, higher PRF allows to obtain better SNR, since the high-frequency contributions are lower in power, as shown in Fig. 7. Increasing the baseline and PRF pushes the system towards ill-conditioning, as predicted by Figure 5. Thus, one should carefully tune the parameters, taking into account the possible values of the slope, incident angle and slant range.

5. CONCLUSIONS

This paper provides an extension to the known multi-channel spectrum reconstruction algorithm, accounting for a constant slope in topography. The inverse system is able to compensate the phase difference imposed by topography and suppress ambiguities. The approach advances from the flat earth paradigm used in most of the current SIMO recombination techniques.

Results obtained under the two major approximations of (1) monodimensional acquisition (i.e. coarse range resolution) and (2) constant slope along-track are rather good and promising for the extension to a general case of smoothly space-varying topography.

6. REFERENCES

[1] Jean-Paul Aguttes, "Formations oriented along the path of SAR satellites," Dec. 2003.

[2] Zhenfang Li, Hongyang Wang, Tao Su, and Zheng Bao, "Generation of wide-swath and high-resolution SAR images from multichannel small spaceborne SAR systems," *IEEE Geoscience and Remote Sensing Letters*, vol. 2, no. 1, pp. 82–86, Jan. 2005, Conference Name: IEEE Geoscience and Remote Sensing Letters.

[3] Josef Mittermayer, Paco Lopez-Dekker, Thomas Kraus, and Gerhard Krieger, "Small Satellite Dispersed SAR - an Exemplary Configuration," in *Proceedings of EUSAR 2016: 11th European Conference on Synthetic Aperture Radar*, June 2016, pp. 1–4.

[4] Davide Giudici, Pietro Guccione, Marco Manzoni, Andrea Monti Guarnieri, and Fabio Rocca, "Compact and Free-Floating Satellite MIMO SAR Formations," *IEEE Transactions on Geoscience and Remote Sensing*, vol. 60, pp. 1–12, 2022, Conference Name: IEEE Transactions on Geoscience and Remote Sensing.

[5] Nida Sakar, Marc Rodriguez-Cassola, Pau Prats-Iraola, and Alberto Moreira, "Sampling Analysis and Processing Approach for Distributed SAR Constellations With Along-Track Baselines," *IEEE Transactions on Geoscience and Remote Sensing*, vol. 60, pp. 1–12, 2022, Conference Name: IEEE Transactions on Geoscience and Remote Sensing.

[6] Thomas Kraus, Gerhard Krieger, Markus Bachmann, and Alberto Moreira, "Addressing the Terrain Topography in Distributed SAR Imaging," in *2019 International Radar Conference (RADAR)*, Sept. 2019, pp. 1–5, ISSN: 2640-7736.

[7] Ozan Dogan, Faruk Uysal, and Paco Lopez Dekker, "Unambiguous Recovery of Multistatic SAR Data for Nonzero Cross Track Baseline Case," *IEEE Geoscience and Remote Sensing Letters*, vol. 19, pp. 1–5, 2022, Conference Name: IEEE Geoscience and Remote Sensing Letters.

[8] Haoyu Lin, Yunkai Deng, Heng Zhang, Da Liang, and Xiaoxue Jia, "An Imaging Method for Spaceborne Cooperative Multistatic SAR Formations With Nonzero Cross-Track Baselines," *IEEE Journal of Selected Topics in Applied Earth Observations and Remote Sensing*, vol. 15, pp. 8541–8551, 2022, Conference Name: IEEE Journal of Selected Topics in Applied Earth Observations and Remote Sensing.